Analysis of Rayleigh-Brillouin spectral profiles and Brillouin shifts in nitrogen gas and air

Yong Ma,[1] Hao Li,[1] ZiYu Gu,[2] Wim Ubachs,[2] Yin Yu,[1] Jun Huang,[1] Bo Zhou,[1] Yuanqing Wang,[1] and Kun Liang[1,*]

[1]*Department of Electronics and Information Engineering, Huazhong University of Science and Technology,Wuhan, 430074, China*

[2]*Department of Physics and Astronomy, LaserLaB, VU University, De Boelelaan 1081, 1081 HV Amsterdam, The Netherlands*

**liangkun@hust.edu.cn*

Abstract: On the basis of experimental Rayleigh-Brillouin scattering data in gaseous nitrogen and air, simulations are performed to describe the observed frequency profiles in analytical form. The experimental data pertain to a $\lambda =$ 366 nm scattering wavelength, a 90° scattering angle, pressures of 1 and 3 bar, and temperatures in the range 250 – 340 K. Two different models are used to represent the RB-profiles, to distinguish the RB-peaks, and to obtain the Brillouin shift associated with the acoustic waves generated in a gaseous medium. Calculations in the framework of V3 and G3 models, exhibiting composite profiles of three distinct peaks of Voigt or Gaussian functions, are compared to observation. Fitting results show that the V3 model yields an improvement over the G3 model. This mathematical model provides an even better representation of the observed profiles than the Tenti S6 model, which is considered to be the optimum representation in terms of physical parameters. For the derivation of Brillouin shifts, both models perform well at high gas pressure, while at lower pressures, the V3 model yields a higher accuracy than the G3 model.

OCIS codes: (010.1310) Atmospheric scattering; (290.5830) Scattering, Brillouin; (290.5870) Scattering, Rayleigh

References and links

1. R. D. Mountain, "Spectral distribution of scattered light in a simple fluid," Rev. Mod. Phys. **38**(1), 205–214 (1966).
2. X. Bao and L. Chen, "Recent progress in Brillouin scattering based fiber sensors," Sensors (Basel) **11**(12), 4152–4187 (2011).
3. S. Xie, M. Pang, X. Bao, and L. Chen, "Polarization dependence of Brillouin linewidth and peak frequency due to fiber inhomogeneity in single mode fiber and its impact on distributed fiber Brillouin sensing," Opt. Express **20**(6), 6385–6399 (2012).
4. E. Fry, J. Katz, D. Liu, and T. Walther, "Temperature dependence of the Brillouin linewidth in water," J. Mod. Opt. **49**(3-4), 411–418 (2002).
5. K. Schorstein, E. S. Fry, and T. Walther, "Depth-resolved temperature measurements of water using the Brillouin lidar technique," Appl. Phys. B **97**(4), 931–934 (2009).
6. J. Huang, Y. Ma, B. Zhou, H. Li, Y. Yu, and K. Liang, "Processing method of spectral measurement using F-P etalon and ICCD," Opt. Express **20**(17), 18568–18578 (2012).
7. J. Shi, Y. Tang, H. Wei, L. Zhang, D. Zhang, J. Shi, W. Gong, X. He, K. Yang, and D. Liu, "Temperature dependence of threshold and gain coefficient of stimulated Brillouin scattering in water," Appl. Phys. B **108**(4), 717–720 (2012).
8. B. Witschas, M. O. Vieitez, E. J. van Duijn, O. Reitebuch, W. van de Water, and W. Ubachs, "Spontaneous Rayleigh-Brillouin scattering of ultraviolet light in nitrogen, dry air, and moist air," Appl. Opt. **49**(22), 4217–4227 (2010).
9. Z. Gu and W. Ubachs, "Temperature-dependent bulk viscosity of nitrogen gas determined from spontaneous Rayleigh-Brillouin scattering," Opt. Lett. **38**(7), 1110–1112 (2013).
10. Z. Gu, M. O. Vieitez, E. J. van Duijn, and W. Ubachs, "A Rayleigh-Brillouin scattering spectrometer for ultraviolet wavelengths," Rev. Sci. Instrum. **83**(5), 053112 (2012).

#199082 - $15.00 USD Received 7 Oct 2013; accepted 14 Jan 2014; published 24 Jan 2014

11. L. Zou, X. Bao, S. Afshar V, and L. Chen, “Dependence of the Brillouin frequency shift on strain and temperature in a photonic crystal fiber,” Opt. Lett. **29**(13), 1485–1487 (2004).
12. K. Schorstein, A. Popescu, M. Gobel, and T. Walther, “Remote water temperature measurements based on Brillouin scattering with a frequency-doubled pulsed Yb:doped fiber amplifier,” Sensors (Basel Switzerland) **8**(9), 5820–5831 (2008).
13. K. Liang, Y. Ma, J. Huang, H. Li, and Y. Yu, “Precise measurement of Brillouin scattering spectrum in the ocean using F–P etalon and ICCD,” Appl. Phys. B **105**(2), 421–425 (2011).
14. K. Liang, Y. Ma, Y. Yu, J. Huang, and H. Li, “Research on simultaneous measurement of ocean temperature and salinity using Brillouin shift and linewidth,” Opt. Eng. **51**(6), 066002 (2012).
15. J. Xu, X. Ren, W. Gong, R. Dai, and D. Liu, “Measurement of the bulk viscosity of liquid by Brillouin scattering,” Appl. Opt. **42**(33), 6704–6709 (2003).
16. D. Liu, J. Xu, R. Li, R. Dai, and W. Gong, “Measurements of sound speed in the water by Brillouin scattering using pulsed Nd:YAG laser,” Opt. Commun. **203**(3-6), 335–340 (2002).
17. A. Griffin, “Brillouin light scattering from crystals in the hydrodynamic region,” Rev. Mod. Phys. **40**(1), 167–205 (1968).
18. R. D. Mountain, “Thermal relaxation and Brillouin scattering in liquids,” J. Res. Natl. Bur. Stand. Sect. A **70A**(3), 207–220 (1966).
19. Q. Zheng, “On the Rayleigh-Brillouin scattering in air,” PhD thesis, University of New Hampshire (2004).
20. G. Tenti, C. D. Boley, and R. C. Desai, “On the kinetic model description of Rayleigh-Brillouin scattering from molecular gases,” Can. J. Phys. **52**(4), 285–290 (1974).
21. C. Boley, R. Desai, and G. Tenti, “Kinetic models and Brillouin scattering in a molecular gas,” Can. J. Phys. **50**(18), 2158–2173 (1972).
22. B. Witschas, “Analytical model for Rayleigh-Brillouin line shapes in air,” Appl. Opt. **50**(3), 267–270 (2011).
23. X. Pan, P. F. Barker, A. Meschanov, J. H. Grinstead, M. N. Shneider, and R. B. Miles, “Temperature measurements by coherent Rayleigh scattering,” Opt. Lett. **27**(3), 161–163 (2002).
24. Y. Ma, F. Fan, K. Liang, H. Li, Y. Yu, and B. Zhou, “An analytical model for Rayleigh–Brillouin scattering spectra in gases,” J. Opt. **14**(9), 095703 (2012).
25. Z. Gu, B. Witschas, W. van de Water, and W. Ubachs, “Rayleigh-Brillouin scattering profiles of air at different temperatures and pressures,” Appl. Opt. **52**(19), 4640–4651 (2013).
26. J. P. Boon and S. Yip, *Molecular Hydrodynamics*, (McGraw-Hill, 1980).
27. C. D. Geisler and S. Greenberg, “A two-stage nonlinear cochlear model possesses automatic gain control,” J. Acoust. Soc. Am. **80**(5), 1359–1363 (1986).
28. G. S. K. Wong and T. F. W. Embleton, “Variation of specific heats and of specific heat ratio in air with humidity,” J. Acoust. Soc. Am. **76**(2), 555–559 (1984).

1. Introduction

Rayleigh scattering refers to the central peak in the spectral profile for light scattering in a medium. Although this feature is commonly viewed as elastic, even this central part of the profile is composed of a distribution of frequency components resulting from the velocity distribution of the molecules or atoms, known as Doppler effect and represented by a purely Gaussian function. The width of this Gaussian depends on the scattering angle and collapses in the forward direction into a delta function. Brillouin scattering, on the other hand, is caused by the energy exchange between light and acoustic modes in the medium, or in a quantum point of view between photons and phonons. Therefore, this scattering gives rise to two side-peaks, Stokes and anti-Stokes shifted from the center, known as the Brillouin shift. In gaseous media of not too high pressures both features are overlapped and the scattering process is described as Rayleigh-Brillouin scattering [1].

In recent years, the study of Rayleigh-Brillouin scattering (RBS) has been applied to determine the physical properties of transparent media, such as optical fibers [2, 3], water [4–7], and gas [8–10]. In these applications, the Brillouin shift plays an important role in the measurement as it has relations with the material properties of the medium. Bao et al. [2, 11] showed that the strain and temperature of optical fibers can be measured by the Brillouin shift, and an optical sensor based on this method has found widespread application. In oceanographic studies it has been demonstrated that the Brillouin shift can be obtained from Lidar-based RBS of the ocean surface, where it can be used for remote sensing of the ocean temperature [12, 13], salinity [14], viscosity [15] and sound speed [16].

So far, no detailed studies have demonstrated the measurement of material properties of a gaseous substance by the Brillouin shift. This is because the contributions of the central Rayleigh peak and the Brillouin side peaks in light scattering from a gas become mixed, at least at atmospheric pressures. Hence, the actual value of the Brillouin shift is difficult to derive from composite three-peak scattering profiles. In contrast, in the hydrodynamic regime, reached in the high-density environment of solid, liquid, and high-pressure gaseous media [17, 18], the central Rayleigh peak and the Brillouin side peaks become significantly separated from each other [13]. Under these conditions, the Brillouin shift can be determined straightforwardly. For gaseous media, where RBS occurs in the kinetic regime ($0.05 < y < 5$, with y a dimensionless parameter defined as the ratio of scattering wavelength to the mean free path) [19] Rayleigh and Brillouin peaks (including Stokes and anti-Stokes) overlap considerably and are more difficult to disentangle. Since the Brillouin shift cannot be obtained directly from experiment, the characterization of gaseous properties from RB-scattering is limited.

Current methods for characterizing the thermodynamic properties of a gaseous medium are based on the composite RBS spectrum. The Tenti model in its S6 [20] and S7 [21] variants are recognized as the best physical models to describe the RBS line shape directly in terms of the macroscopic transport coefficients of a gas that can be measured independently by various means. Therefore, the RBS spectral profile can be calculated from the known gas parameters. However, in applications such as remote sensing of the atmosphere, the purpose is often to use a rapid algorithm for deriving thermodynamic properties of a medium such as pressure or temperature. In such case, use of S6 or S7 models is complicated and time consuming, since these models are not represented in analytical form [22]. Therefore an alternative or simplified model in analytical form would provide a rapid and fruitful tool to be used in satellite retrieval extracting gaseous properties of atmospheres on-line.

As for an analytical model, a single-Gaussian model [23] has a simple functional form and is quite easy to implement, but it yields only an imprecise approximation of the RBS spectrum and large errors will result [24]. In 2011, Witschas [22] proposed an analytical model involving a composite spectrum of three Gaussians (henceforth named "G3" for convenience) for the RBS line shape in air, and proved that it is well applicable for a range of dimensionless scattering parameters $y = 0 – 1$. In a previous study of the Wuhan group from 2012 [24] a "V3" model was developed, where the composite spectrum is composed of three peaks represented by an analytical pseudo-Voigt function. Both models are capable of analytically separating the Rayleigh and Brillouin peaks. For the V3 model it was shown to cover a wider parameter space ($y = 0$ - 4) and to remain closer to the S6 and S7 model descriptions.

In [22, 24] comparisons were made between G3 and V3 analytical models and the Tenti S6 and S7 model, that describe RB-scattering in physical terms, although some approximations are made in the derivation of S6 and S7 models. In the present study, a direct comparison is made between G3 and V3 analytical models and experimental data on RB-scattering for N_2 and air [9, 25]. Both V3 and G3 models are fitted to the experimental data, and the fitting results are subsequently compared with the S6 model. The V3 and G3 models are utilized to distinguish Rayleigh and Brillouin peaks to obtain experimental values for the Brillouin shift, which may then be confronted with values calculated from thermodynamic gas properties.

2. RBS theory and analytical models of the line profile

Rayleigh–Brillouin scattering (RBS) manifests itself as two features: a Doppler-broadened central Rayleigh peak and two Stokes and anti-Stokes shifted Brillouin peaks. As the frequency shift of the two Brillouin peaks is relatively small for gases, they overlap with the Rayleigh peak and form a mixed profile. The RBS line shape can be viewed as a linear combination of the Rayleigh peak and the Brillouin doublet, where each part can be described independently by a functional form.

In 2011, Witschas [22] has proposed an analytical model for RBS based on combinations of three Gaussian profiles, as follows:

#199082 - $15.00 USD Received 7 Oct 2013; accepted 14 Jan 2014; published 24 Jan 2014

$$G(v)=\frac{1}{\sqrt{2\pi}\Gamma_R}A\cdot\exp\left[-\frac{1}{2}\left(\frac{v}{\Gamma_R}\right)^2\right]+\frac{1-A}{2\sqrt{2\pi}\Gamma_B}\cdot\exp\left[-\frac{1}{2}\left(\frac{v+v_B}{\Gamma_B}\right)^2\right]+\frac{1-A}{2\sqrt{2\pi}\Gamma_B}\cdot\exp\left[-\frac{1}{2}\left(\frac{v-v_B}{\Gamma_B}\right)^2\right] \quad (1)$$

where v is the frequency of the incident light source, A is a parameter representing the spectral intensity, v_B is the Brillouin shift, and Γ_R and Γ_B are the linewidths of the Rayleigh peaks and Brillouin peaks, respectively. In this model Rayleigh and Brillouin peaks are treated as Gaussian, and the modeled spectrum is a combination of three Gaussian profiles. This description is referred to as the G3 model. This approach was demonstrated to produce an accurate description of the RBS profile under gaseous conditions of low y-parameters, in the range 0 - 1 [22].

The line shapes of both Rayleigh and Brillouin scattering will be affected by homogeneous and inhomogeneous broadening effects, with the former having a Lorentzian line shape and the latter a Gaussian line shape [13, 19]. In 2012, some of the present authors developed a V3 model to analyze the composition of the RBS spectrum in analytical form. Based on line broadening theory, the line shapes of both Rayleigh and Brillouin scattering were expressed as pseudo-Voigt profile functions $V(v)$ [24]:

$$V(v)=\rho\cdot L(v;\Gamma_L,v_L)+(1-\rho)\cdot G(v;\Gamma_G,v_L) \quad (2)$$

where ρ $(0 < \rho < 1)$ is a parameter representing the proportion of the Lorentzian profile in the pseudo-Voigt profile, $L(v; \Gamma_L, v_L)$ representing a Lorentzian and $G(v; \Gamma_G, v_G)$ a Gaussian profile, respectively:

$$G(v;\Gamma_G,v_G)=\frac{2\sqrt{\ln 2}}{\sqrt{\pi}\cdot\Gamma_G}\cdot\exp\left\{\frac{-4\ln 2\cdot(v-v_G)^2}{\Gamma_G{}^2}\right\} \quad (3)$$

$$L(v;\Gamma_L,v_L)=\frac{2}{\pi}\cdot\frac{\Gamma_L}{4(v-v_L)^2+\Gamma_L{}^2} \quad (4)$$

Here Γ_G and v_G are the width and center frequency of the Gaussian profile, Γ_L and v_L the width and center frequency of the Lorentzian profile. The RBS spectrum contains one Rayleigh peak and two Brillouin peaks, and the analytical form of V3 model can be expressed as the linear combination of three pseudo-Voigt profiles:

$$V_{RB}=\mathbf{C}^T\cdot\{Diag(\boldsymbol{\rho})\cdot\mathbf{G}+[\mathbf{I_3}-Diag(\boldsymbol{\rho})]\cdot\mathbf{L}\} \quad (5)$$

where, $\mathbf{C} = [A\ B\ B]^T$, A stands for the weight factor of the Rayleigh portion, and B for the weight factor of the Brillouin portion; $\mathbf{I_3}$ is the identity matrix of order 3, $\mathbf{G} = [G_{Rayl}(v)\ G^{+}_{Brill}(v)\ G^{-}_{Brill}(v)]^T = [G(v; \Gamma_{GR}, 0)\ G(v; \Gamma_{GB}, -v_B)\ G(v; \Gamma_{GB}, -v_B)]^T$ is the Gaussian component in the three peaks, v the functional coordinate of the RBS spectrum, Γ_{GR} and Γ_{GB} are the Gaussian linewidths of the Rayleigh peak and Brillouin peaks, respectively; $\mathbf{L} = [L_{Rayl}(v)\ L^{+}_{Brill}(v)\ L^{-}_{Brill}(v)]^T = [L(v; \Gamma_{LR}, 0)\ L(v; \Gamma_{LR}, -v_B)\ L(v; \Gamma_{Lr}, -v_B)]^T$ is the Lorentzian component in the three peaks, Γ_{LR} and Γ_{LB} are the widths of the Lorentzian components of the Rayleigh and Brillouin peaks, respectively; $\boldsymbol{\rho} = [\rho_R\ \rho_B\ \rho_B]^T$ is a column vector for the Lorentzian proportions of the three peaks. The composite profile is centered around $\nu = 0$, and v_B is the Brillouin shift. In this model, the undetermined parameters are in the vectors **C**, **G**, **L**, **ρ**. All undetermined parameters indicate certain features of Rayleigh peak and Brillouin peaks. By using V3 model fitting to experimental or simulated data for an RBS spectrum, these parameters can be obtained.

Unlike the non-analytical Tenti S6 and S7 models, both V3 and G3 models are cast in analytical forms and explicitly contain the Brillouin shift. Therefore, a value for the Brillouin shift v_B can be obtained via direct least-squares fitting to an experimental RBS spectrum. In the next section, the V3 model and G3 models will be compared with experimental RBS data for N_2 and air [9, 25], and in each case the Brillouin shift will be determined. Finally, by evaluating the fitting errors of both models and the accuracy of the obtained Brillouin shift, the usefulness of both models to derive physical properties from RB scattering is assessed.

3. Experimental data

The experimental data were obtained in a Rayleigh-Brillouin spectrometer, designed for measuring RBS proðles at 366 nm with an effective power of 5W [10]. The scattered lighted is collected at 90° with an uncertainty of 0.9°. The value of the scattering angle can be determined at improved accuracy of less than 0.1° by comparing the experimental scattering data to the S6 model [25], because the width of the overall scattering profile is very sensitive to the angle. The RB-scattered light is spectrally filtered by a Fabry-Perot Interferometer (FPI) with an instrument linewidth of 232 MHz and a free spectral range of 7440 MHz, before detection.

Experimentally, RB-scattering was measured in air and in pure nitrogen gas at two different charging pressures: 1 bar and 3 bar. Note that the actual pressures, measured on a baratron in the experiment, deviate somewhat from these values. For each pressure measurements were performed at a number of different temperatures covering the range 250 – 340 K. Table 1 shows the pressure and temperature conditions at which data were collected; the scattering angles, derived from the profiles are indicated as well.

Table 1. Gas conditions and the scattering angles for the RBS experiments

	1 bar condition			3 bar condition		
	Temperature (K)	Pressure (bar)	Scattering angle	Temperature (K)	Pressure (bar)	Scattering angle
Air	254.8	0.858	90.0°	255.0	2.576	89.7°
	276.7	0.947	90.3°	278.0	2.813	89.3°
	297.3	1.013	90.4°	297.6	2.910	89.7°
	318.3	1.013	90.4°	319.3	3.128	89.7°
	337.8	1.017	90.5°	337.7	3.304	89.8°
Nitrogen	256.0	0.862	89.7°	254.7	2.563	89.4°
	275.0	0.940	89.6°	275.2	2.784	89.5°
	296.7	1.010	89.7°	296.7	3.000	89.6°
	336.0	1.140	89.8°	336.6	3.400	89.6°

4. Analysis

The experimental data, reported previously in [9] and [25], are included in V3 and G3 model analyses with the aim to generate an optimally fitting profile description and determination of the Brillouin shift. In Figs. 1, 2, 3 and 4, both the V3 and the G3 models, convolved with the instrument function (Airy function) of the FPI, are compared with the RBS spectra at 1 bar air and 1 bar nitrogen at different temperature conditions (marked in the figures), respectively.

The residuals plotted in Figs. 1-4 show that both V3 and G3 models fit the experimental RBS spectra well. The rms noise, which is the standard deviation of the noise distribution, is at the 0.5% level (percentages given with respect to peak intensity) for the V3 model and at the 1% level for the G3 model. Moreover, the V3 model has slightly better fitting results as the deviations between the measurement and the modeling calculation display statistical fluctuations without structure, while the deviation of G3 model displays some systematic oscillations at the 1% level It is worth noting that such systematic deviations are also observed in comparison with the S6 model [25].

#199082 - $15.00 USD Received 7 Oct 2013; accepted 14 Jan 2014; published 24 Jan 2014

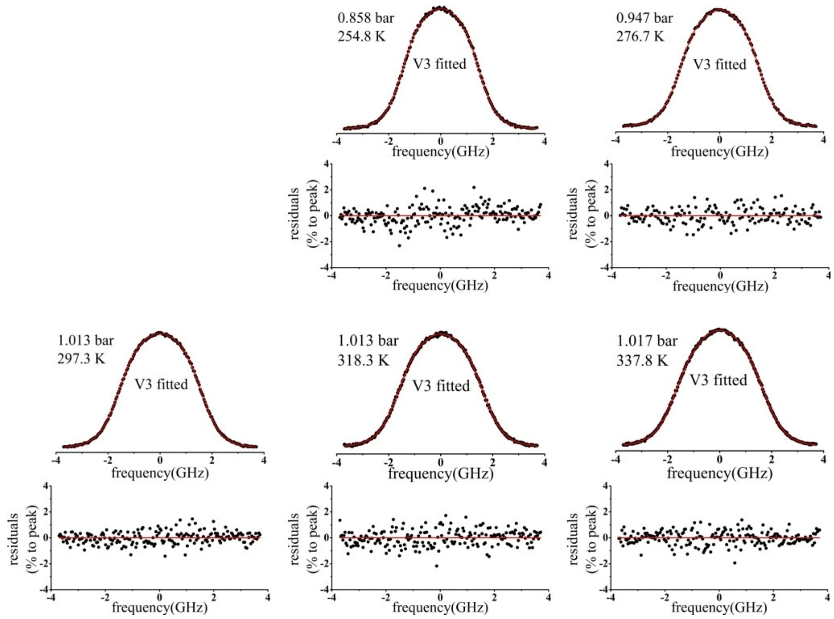

Fig. 1. Model description for the RBS spectrum of 1 bar air with the V3 model under different temperature conditions as indicated. Fitted curves are shown with red lines and the experimental RBS spectrum as black dots; lower panels show the residuals between experiment and model description.

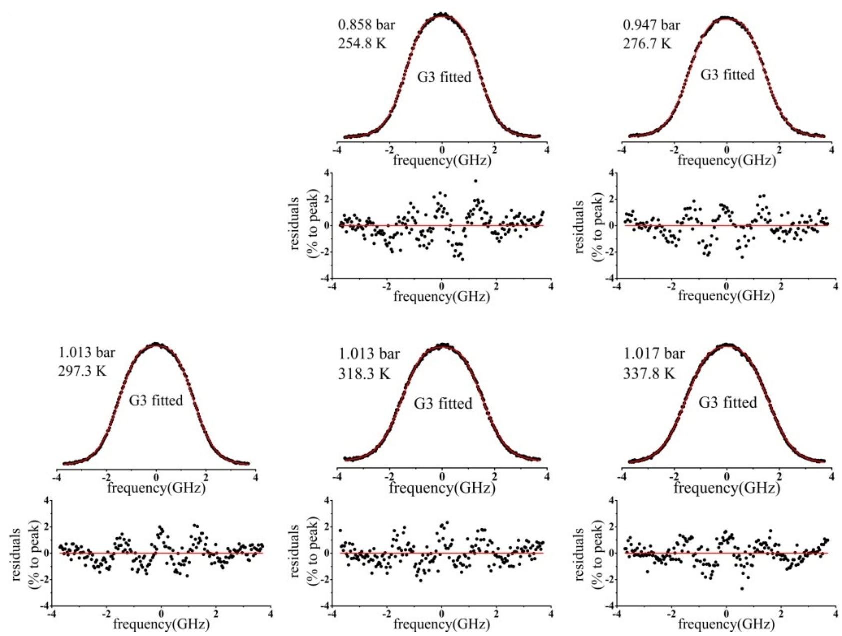

Fig. 2. Model description for the RBS spectrum of 1 bar air with the G3 model under different temperature conditions as indicated. Fitted curves are shown with red lines and the experimental RBS spectrum as black dots; lower panels show the residuals between experiment and model description.

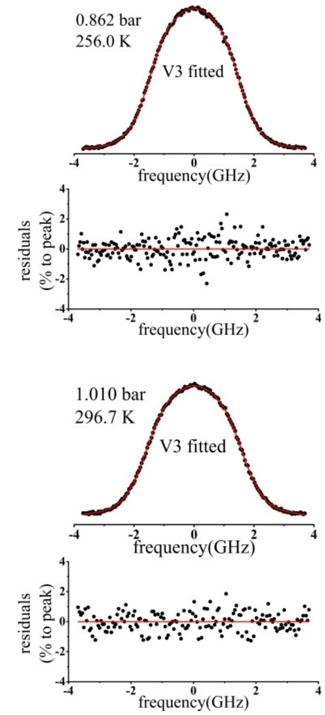

Fig. 3. Results for 1 bar N_2 gas for the V3 model.

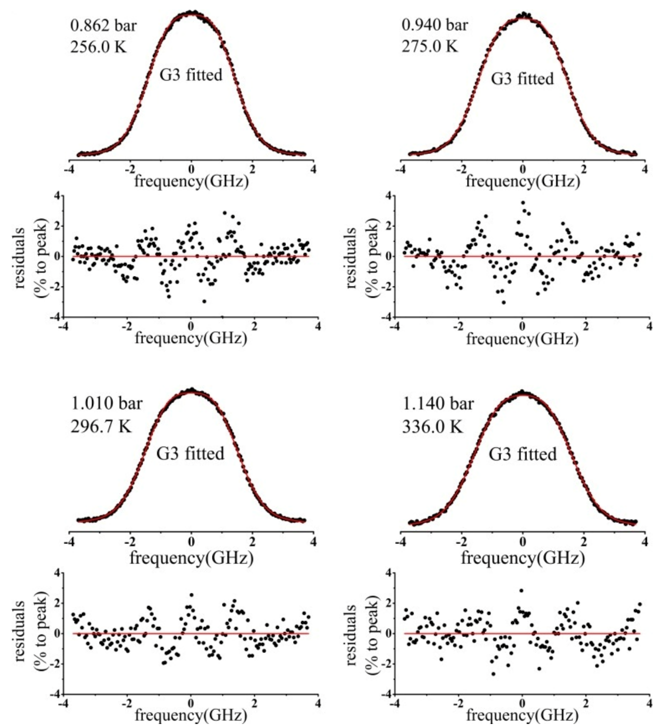

Fig. 4. Results for 1 bar N_2 gas for the G3 model.

In order to present a more detailed comparison, the root-mean-square error (RMSE) and the χ^2 of the fittings of air and nitrogen RBS spectrum are shown in Figs. 5(a)-5(b) and Figs. 6(a)-6(b), respectively. The RMSE and $\chi^2$are calculated as follows:

$$RMSE = \sqrt{\frac{\sum_{i=1}^{N}[I_e(f_i) - I_m(f_i)]^2}{N}} \tag{6}$$

$$\chi^2 = \frac{1}{N}\sum_{i=1}^{N}\frac{[I_e(f_i) - I_m(f_i)]^2}{\sigma^2(f_i)} \tag{7}$$

where $I_e(f_i)$ and $I_m(f_i)$ are the experimental and modeled amplitude of the spectrum at frequency f_i, and $\sigma(f_i)$ is the statistical (Poisson) error, including effects of background and dark count rate. As the S6 model is known as the best physical model to describe a spontaneous RBS spectrum in the kinetic regime, the RMSE and χ^2 values from comparison with the S6 model reported in [25] are also added in the figures.

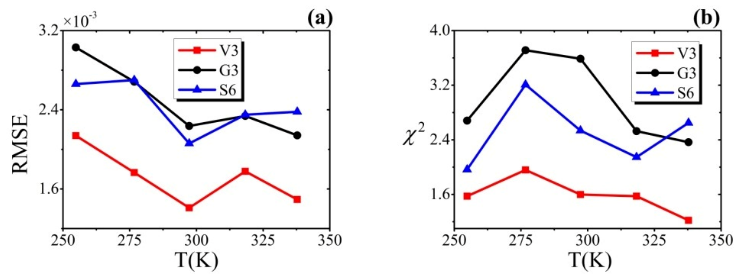

Fig. 5. The RMSE values (a) and the χ^2 values (b) for V3, G3, and S6 models for conditions of 1 bar air.

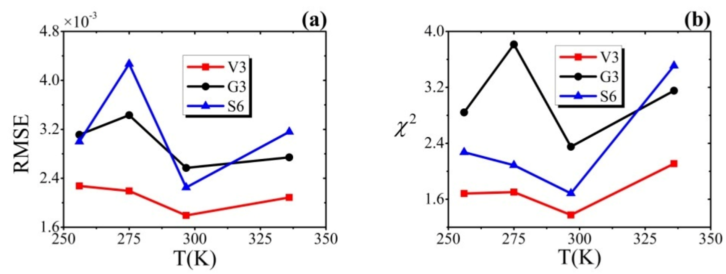

Fig. 6. The RMSE values (a) and the χ^2 values (b) for V3, G3, and S6 models for conditions of 1 bar nitrogen.

It can be seen from Figs. 5(a)-5(b) and Figs. 6(a)-6(b) that for the same experimental data set, all three models tend to have lower RMSE/χ^2 values at certain temperature (e.g. 296.7 K and 1 bar N_2) and higher RMSE/χ^2 values at other temperatures (e.g. 336.0 K and 1 bar N_2), while both RMSE and χ^2 values of V3 are the lowest in any condition. Therefore it can be concluded that among the three models, the V3 model has the best fitting goodness. It is interesting to note that although the V3 and S6 models serve different purposes, from a modeling perspective the V3 model agrees with the experiment better than the S6 model according to Figs. 5(a)-5(b) and Figs. 6(a)-6(b). This may be explained from the fact the V3 model contains a large number of free parameters fitted to the experimental data. In contrast, comparisons with the Tenti S6 model involve macroscopic transport coefficients, which are usually not fitted but adopted as known material properties of the gas, except for the elusive bulk viscosity, which is fitted in some cases [9, 25].

For the data set recorded at pressures of 3 bar, similar results are presented. Figures 7, 8, 9, and 10 show the fitting results for the RBS spectra of 3 bar air and 3 bar nitrogen, respectively. Again fitting to experimental data is performed using the V3 model and the G3 model for all pressure and temperature conditions. The root-mean-square error (RMSE) and the χ^2 values for the fitting of the air and nitrogen RBS spectrum are shown in Figs. 11(a)-11(b) and Figs. 12(a)-12(b).

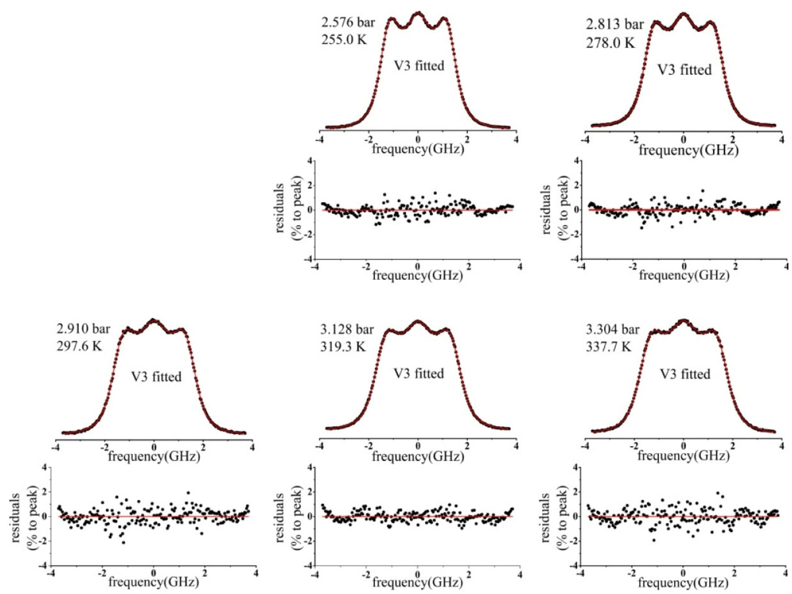

Fig. 7. Model description for the RBS spectrum of 3 bar air with the V3 model under different temperature conditions as indicated. Fitted curves are shown with red lines and the experimental RBS spectrum as black dots; lower panels show the residuals between experiment and model description.

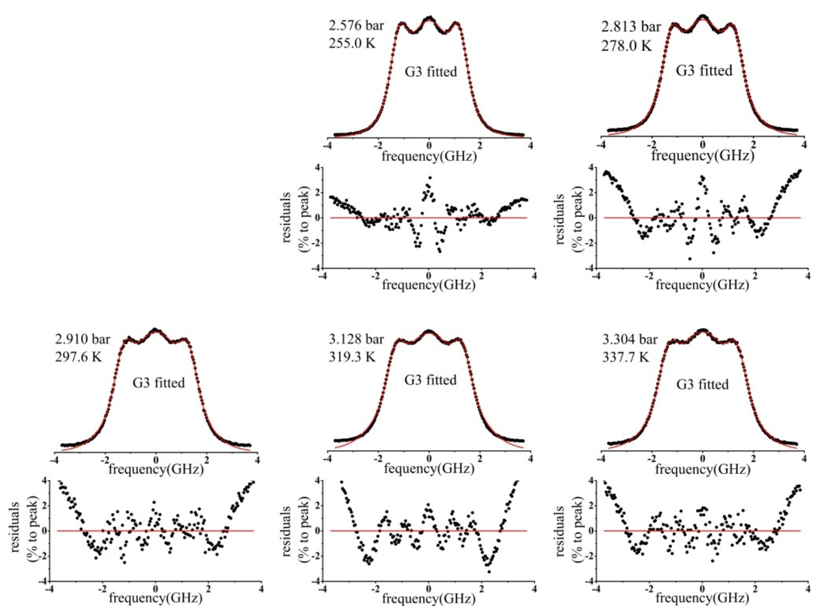

Fig. 8. Model description for the RBS spectrum of 3 bar nitrogen with the G3 model under different temperature conditions.

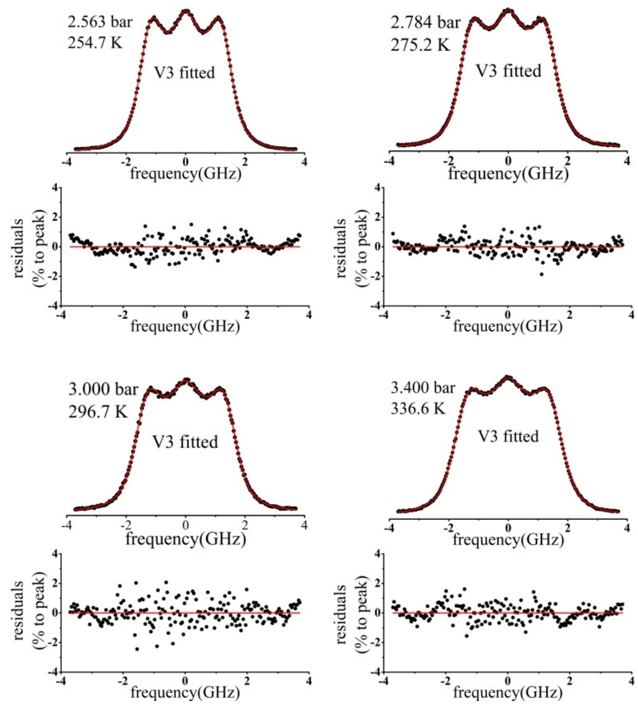

Fig. 9. Model description for RBS at 3 bar nitrogen with the V3 model under different temperature conditions.

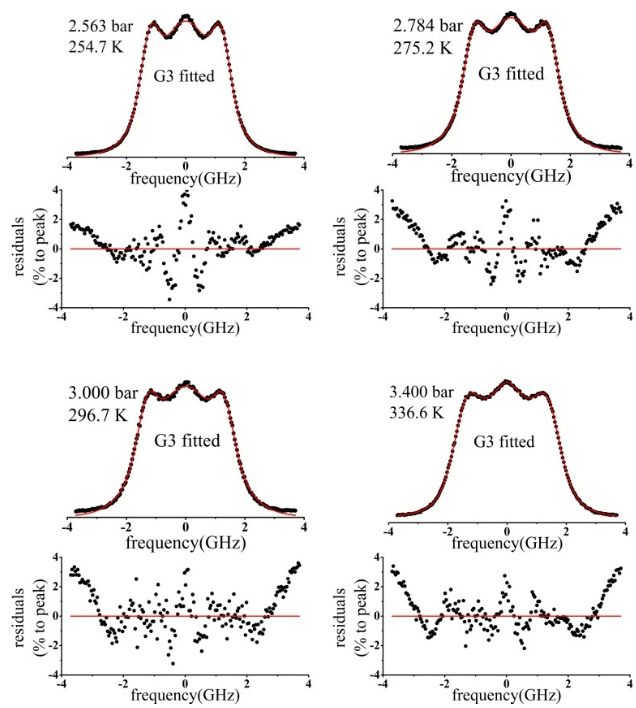

Fig. 10. Model description for RBS at 3 bar nitrogen with the G3 model under different temperature conditions.

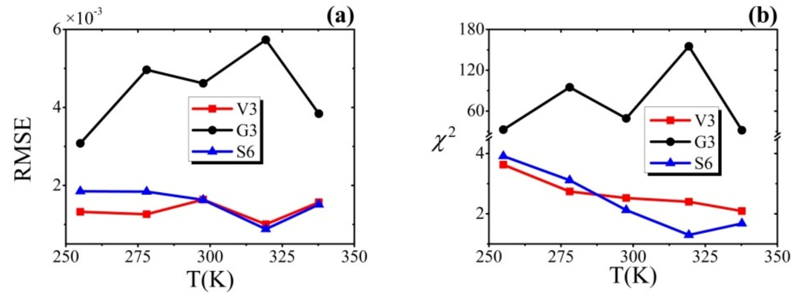

Fig. 11. The RMSE values (a) and the χ^2 values (b) for V3, G3, and S6 models for conditions of 3 bar air.

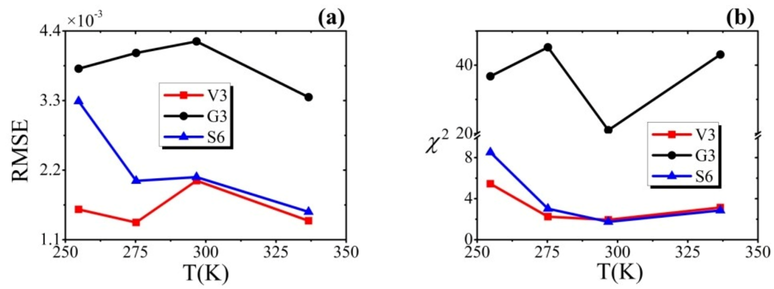

Fig. 12. The RMSE values (a) and the χ^2 values (b) for V3, G3, and S6 models for conditions of 3 bar nitrogen.

Compared with conditions of 1 bar, the rms noise for conditions of 3 bar is reduced to less than 0.5% for the V3 model, but increases to more than 1% for the G3 model. For the residuals in Fig. 7 to Fig. 10, systematic oscillatory deviations for the V3 model remain absent, while the G3 model yields systematic oscillations at the 2% level. Compared with the 1% rms noise level and the 2% deviation reported in [25], the V3 model also reproduces the experimental data slightly better than the S6 model for conditions of 3 bar. In Figs. 11(a)-11(b) and Figs. 12(a)-12(b) it is demonstrated that the RMSE and χ^2 values for the V3 model are still slightly better than those of S6 model at most temperatures, while the fitting values for G3 are much worse.

The reason for the improvement resulting from the V3 model representing the data for 3 bar is that, unlike the smooth curve under 1 bar pressure conditions, the RBS spectrum at 3 bar displays pronounced Brillouin shoulders. As a result, the RBS spectrum at 3 bar will be more constrained in the fitting procedure. On the other hand, Witschas pointed out [22] that the G3 model is well applicable for $y = [0, 1]$, but less so for the range $y = 1.6 \sim 1.7$, here covered by gas pressures of 3 bar. The improved goodness-of-fit for the V3 model for the higher pressure regime can intuitively be understood from the fact that the Rayleigh-Brillouin profile in the hydrodynamic regime will take the form of Lorentzian profiles [26]. Hence at the higher pressures in the intermediate regime the Lorentzian components, associated with the homogeneous broadening effects due to collisions, will gain in importance, for which reason the V3 model will yield a better description of the RB scattering profiles.

5. Derivation of the Brillouin shift

To verify the performance of the V3 model in measurements of the Brillouin shift, the accuracy of the acquired Brillouin shift via various methods will be evaluated. In order to evaluate the measurement accuracy of the Brillouin shift, the values of the Brillouin shift v_{bt} are predicted as [9]:

#199082 - \$15.00 USD Received 7 Oct 2013; accepted 14 Jan 2014; published 24 Jan 2014
(C) 2014 OSA 27 January 2014 | Vol. 22, No. 2 | DOI:10.1364/OE.22.002092 | OPTICS EXPRESS 2102

$$\nu_{bt} = \frac{2n}{\lambda} \cdot \nu_S \cdot \sin(\theta / 2) \tag{8}$$

where n is the refractive index of the gas, θ is the scattering angle and ν_S is the sound speed in the gas, which is related to the physical parameters of the gas [27, 28]:

$$\nu_s = \sqrt{\gamma \cdot R \cdot T / m} \tag{9}$$

with γ the adiabatic constant, R the universal gas constant, T the absolute temperature of the gas in Kelvin, and m the molecular weight of the gas. The parameters for air and nitrogen are as follows: γ = 1.4, R = 8.314 J·mol^{-1}·K^{-1}, the molecular weight of the air m_A = 28.964 × 10^{-3} kg·mol^{-1}, and that of nitrogen m_N = 28.014 × 10^{-3} kg·mol^{-1}. The pressures and temperatures are the same as shown in Figs. 1, 2, 3, 4, 7, 8, 9 and 10.

Tables 2 and 3 show the values ν_{bm} fitted from the experimental RBS data using V3 and G3 models, the predicted values ν_{bt}, the error $\Delta\nu$ between ν_{bm} and ν_{bt}, as well as the relative errors $\Delta\nu_r$ for conditions of RBS at 1 bar air and 1 bar nitrogen, respectively.

Table 2. Brillouin shift measured under conditions of 1 bar air, the fitted values ν_{bm} using V3 and G3 models, predicted values ν_{bt}, error $\Delta\nu$ between ν_{bm} and ν_{bt}, as well as relative error $\Delta\nu_r$

T(K)	ν_{bt}(GHz)	V3 model			G3 model		
		ν_{bm}(GHz)	$\Delta\nu$(GHz)	$\Delta\nu_r$(%)	ν_{bm}(GHz)	$\Delta\nu$(GHz)	$\Delta\nu_r$(%)
254.8	1.227	1.111	0.116	9.45%	0.711	0.516	42.05%
276.7	1.281	1.153	0.128	9.99%	0.740	0.541	42.23%
297.3	1.328	1.201	0.127	9.56%	0.765	0.563	42.39%
318.3	1.374	1.235	0.139	10.12%	0.779	0.595	43.30%
337.8	1.415	1.287	0.128	9.05%	0.793	0.622	43.96%

Table 3. Brillouin shift measured under conditions of 1 bar nitrogen, fitted values ν_{bm} using V3 and G3 models, predicted values ν_{bt}, error $\Delta\nu$ between ν_{bm} and ν_{bt}, as well as relative error $\Delta\nu_r$

T(K)	ν_{bt}(GHz)	V3 model			G3 model		
		ν_{bm}(GHz)	$\Delta\nu$(GHz)	$\Delta\nu_r$(%)	ν_{bm}(GHz)	$\Delta\nu$(GHz)	$\Delta\nu_r$(%)
256.0	1.247	1.139	0.108	8.66%	0.727	0.520	41.70%
275.0	1.291	1.205	0.086	6.66%	0.745	0.546	42.29%
296.7	1.341	1.215	0.126	9.40%	0.774	0.567	42.28%
336.0	1.427	1.311	0.116	8.13%	0.810	0.617	43.24%

Resulting relative errors for the V3 model at 1 bar pressure are around 10%, while those for the G3 model are significantly larger (above 40%). Though the V3 and G3 models have similar fitting accuracy, the measurement errors of the Brillouin shifts are widely different.

For the experimental data obtained at 3 bar, similar comparisons of Brillouin shifts fitted with V3 and G3 models result, shown in Tables 4 and 5. It should be noted that the Brillouin shift is not exactly equal to the frequency shift of the side peaks measured at 3 bar.

Table 4. Brillouin shift obtained from experimental data for 3 bar air, fitted values ν_{bm} using V3 and G3 models, predicted values ν_{bt}, error $\Delta\nu$ between ν_{bm} and ν_{bt}, as well as relative error $\Delta\nu_r$

T(K)	ν_{bt}(GHz)	V3 model			G3 model		
		ν_{bm}(GHz)	$\Delta\nu$(GHz)	$\Delta\nu_r$(%)	ν_{bm}(GHz)	$\Delta\nu$(GHz)	$\Delta\nu_r$(%)
255.0	1.224	1.190	0.034	2.78%	1.202	0.022	1.80%
278.0	1.273	1.246	0.027	2.12%	1.252	0.021	1.65%
297.6	1.321	1.292	0.029	2.20%	1.288	0.033	2.41%
319.3	1.367	1.335	0.032	2.34%	1.323	0.044	3.22%
337.7	1.407	1.380	0.027	1.92%	1.375	0.032	2.27%

Table 5. Brillouin shift obtained from experimental for 3 bar nitrogen, fitted values ν_{bm} using V3 and G3 model, predicted values ν_{bt}, Error $\Delta\nu$ between ν_{bm} and ν_{bt}, as well as relative error $\Delta\nu_r$

T(K)	ν_{bt}(GHz)	V3 model			G3 model		
		ν_{bm}(GHz)	$\Delta\nu$(GHz)	$\Delta\nu_r$(%)	ν_{bm}(GHz)	$\Delta\nu$(GHz)	$\Delta\nu_r$(%)
254.7	1.241	1.196	0.045	3.63%	1.218	0.023	1.85%
275.2	1.291	1.261	0.030	2.32%	1.267	0.024	1.86%
296.7	1.340	1.310	0.030	2.24%	1.312	0.028	2.09%
336.6	1.425	1.397	0.028	1.96%	1.396	0.029	2.04%

The data in Tables 4 and 5 show that the fitting accuracy for the Brillouin shift in both V3 and G3 models at 3 bar pressure is about 2% - 4%, which is much better than for the 1 bar condition. The reason is that the RBS spectra at 3 bar pressure, exhibiting more pronounced side features, will impose more constraints on the line shape, and effectively limit the degrees of freedom in the multi-parameter fitting. We also find that in spite of the worse performance in fitting the frequency profile, the Brillouin shifts measured by the G3 model have similar accuracy compared with those measured by the V3 model, and in some cases smaller uncertainties are found. In future studies, this phenomenon will be analyzed with more experimental data. If the accuracy of the Brillouin shift measured via the G3 model is similar to that for the V3 model under high pressure conditions, the G3 model would be sufficient for the Brillouin shift measurement, even though it is not suitable for high pressure RBS spectrum fitting.

In summary, in the analysis of experimental RBS spectra measured at 1 bar pressure, the V3 model allows for a more accurate determination of the Brillouin shift than the G3 model. At 3 bar pressure, the errors obtained by the V3 and G3 models are similar, while the fitting accuracy of the former is significantly better. Therefore when other spectrum characteristics besides the Brillouin width are of interest, a more confident measurement outcome can be expected using the V3 model.

6. Conclusion

In this paper, the Brillouin shift of the RBS spectrum for a gas is obtained from the experimental data for the first time. Two analytical models, the V3 and G3 models, are implemented to fit experimentally obtained RBS spectra of air and N_2 at various temperatures and pressures. The fitting results (including deviations, RMSE and χ^2) showed that the V3 model has the best fitting performance, even better than the Tenti S6 model, which provides a more physically based description of the RB spectral profiles. In addition, V3 proves to be a promising analytical tool to study the gas properties in RBS experiments. It may provide a fast and simple representation of an experimental RBS spectrum in functional form, and as such provide the basis for a rapid algorithm for on-line satellite retrieval of gas phase properties from light scattering.

In deducing a Brillouin shift from experimental data, it is found that the relative errors for V3 and G3 models are around 3% at high gas pressure (3 bar), while at lower gas pressure (1 bar), both models show large deviations with a value predicted from gas transport coefficient, especially the G3 model with a 40% relative error. In comparing the two models, it can be concluded that the V3 model has a wider applicable scope than the G3 model in the RBS spectral fitting.

Acknowledgments

The authors acknowledge the National Natural Science Foundation of China (grant No. 61108074 and 61078062) and the Research Fund for the Doctoral Program of Higher Education of China (grant No. 20100142120012), and the European Space Agency (ESA) for financial support under contract ESTEC-21396/07/NL/HE-CCN-2. Also, the authors would like to thank Dr. B. Witschas (DLR Oberpfaffenhofen, Germany) for helpful discussions.